Prediction of High Resolution Spatial-Temporal Air Pollutant Map from Big Data Sources

Yingyu Li[1], Yifang Zhu[2], Wotao Yin[3], Yang Liu[4], Guangming Shi[1(✉)], and Zhu Han[5]

[1] School of Electronic Engineering, Xidian University, Xi'an, China
yyli.xidian@gmail.com, gmshi@xidian.edu.cn
[2] Department of Environmental Health Sciences, University of California, Los Angeles, USA
yifang@ucla.edu
[3] Department of Mathematics, University of California, Los Angeles, USA
wotaoyin@ucla.edu
[4] Rollins School of Public Health, Emory University, Atlanta, USA
yang.liu@emory.edu
[5] Department of Electrical and Computer Engineering, University of Houston, Houston, USA
zhan2@uh.edu

Abstract. In order to better understand the formation of air pollution and assess its influence on human beings, the acquisition of high resolution spatial-temporal air pollutant concentration map has always been an important research topic. Existing air-quality monitoring networks require potential improvement due to their limitations on data sources. In this paper, we take advantage of heterogeneous big data sources, including both direct measurements and various indirect data, to reconstruct a high resolution spatial-temporal air pollutant concentration map. Firstly, we predict a preliminary 3D high resolution air pollutant concentration map from measurements of both ground monitor stations and mobile stations equipped with sensors, as well as various meteorology and geography covariates. Our model is based on the Stochastic Partial Differential Equations (SPDE) approach and we use the Integrated Nested Laplace Approximation (INLA) algorithm as an alternative to the Markov Chain Monte Carlo (MCMC) methods to improve the computational efficiency. Next, in order to further improve the accuracy of the predicted concentration map, we model the issue as a convex and sparse optimization problem. In particular, we minimize the Total Variant along with constraints involving satellite observed low resolution air pollutant data and the aforementioned measurements from ground monitor stations and mobile platforms. We transform this optimization problem to a Second-Order Cone Program (SOCP) and solve it via the log-barrier method. Numerical simulations on real data show significant improvements of the reconstructed air pollutant concentration map.

Y. Wang et al. (Eds.): BigCom 2015, LNCS 9196, pp. 273–282, 2015.
DOI: 10.1007/978-3-319-22047-5_22

Keywords: Air pollution · High resolution spatial-temporal concentration map · Big data · Heterogeneous data sources · SPDE · INLA · Sparsity · SOCP

1 Introduction

Air pollution is a major environmental risk to our health nowadays. This problem is happening all around the world. Many death-causing diseases, such as lung cancer, stroke, heart disease, and both chronic and acute respiratory diseases, including asthma, are closely related to air pollution . It will become even severe for children and the aged. In 2012, air pollution contributes to around 7,000,000 deaths worldwide [1]. Thus in order to reduce the damage caused by air pollution, it is of vital importance to investigate on its formation and transition process. But the acquisition of high resolution and accuracy air pollutant concentration map has always been a big barrier. Traditional ground monitor stations are one of the main ways to acquire air pollutant concentration information. They can provide accurate air pollutant concentration at specific locations, but the quantity of available information is quite limited, due to the high costs both in human resources and financial resources to run such monitor stations. In recent years, mobile air pollutant sensors [3][4] are becoming more and more popular. They are usually installed on mobile platforms or other public transport vehicles, causing a great reduction in costs. But the available data coverages are still restricted to their trajectories only. Satellites remote sensing techniques can provide the air pollutant concentration information all over their scanned areas, but the spatial and temporal resolutions are low. To summary, it is difficult to acquire high resolution spatial-temporal air pollutant concentration map from a single type of data source.

In order to remedy the limitations in sampling techniques, lots of works have been done to acquire high quality air pollutant concentration maps. Land-Use Regression (LUR) model [4][5][6] is a typical one, which simply assumes that air pollutant concentration is decided by meteorology, climate, geography, human activity and other relative covariates, and then uses regression models to fit the data. In 2013, Zheng et al. [7] proposed a semi-supervised learning approach based on a co-training framework that consists of a spatial classifier and a temporal classifier to predict the air pollution level in a fine defined grid. This method highly improved the prediction accuracy compared to LUR models, but it can only gives the index of air pollution instead of the exact concentration. Cameletti et al. [8][9] further improved the traditional LUR model by adding a spatial-temporal Gaussian field to it, and representing it as a Gaussian Markov Random Field (GMRF) through the Stochastic Partial Differential Equations (SPDE) approach. In order to make the computation more efficient, they also adopted the Integrated Nested Laplace Approximation (INLA) algorithms as an alternative to Markov Chain Monte Carlo (MCMC) sampling. However, the data source used in the above methods are all onefold, which limit their ability to improve the resolution and accuracy of the predicted spatial-temporal air pollutant concentration map.

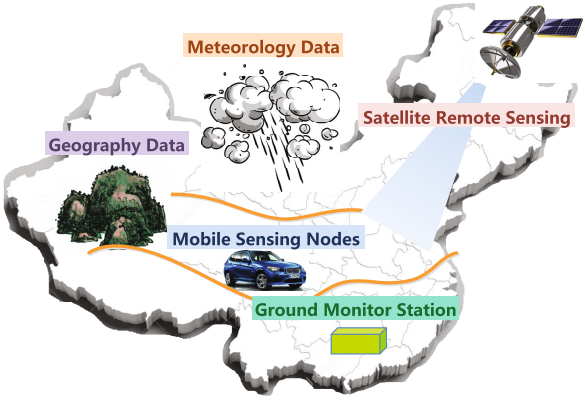

Fig. 1. Illustration of the big data sources used

With the arrival of an era of big data, new opportunities and challenges have been brought to this problem. As we mentioned above, we can have direct measurements from ground monitor stations, mobile platforms with sensing nodes and satellites, as well as many indirect measurements, including various meteorology and geography covariates. These data sources are "big" in both **Variety**, **Volume** and **Velocity**, and construct a typical example of the 3V model in big data techniques [2]. These properties of our data sources can provide us more information about the air pollutant concentration, but also presents new requirements on efficient algorithms and computation methods to handle them.

In this paper, we propose an air pollutant concentration prediction approach that takes advantage of big data sources, including ground monitor stations observed data, mobile platforms with mobile sensing nodes collected data and satellite observed data as shown in Fig.1. Firstly, we use the ground monitor stations observed data as fixed samples and mobile platforms collected data as random samples to predict a preliminary 3D high resolution air pollutant concentration map. The prediction result contains a large scale regression component, where various meteorology and geography covariates are used, and a small scale spatial-temporal process. It is fulfilled via the SPDE approach and solved by the INLA algorithms. In order to further improve the accuracy of the predicted concentration map, we then take satellite observed data into consideration and model the issue as a convex and sparse optimization problem, in which the objective function is built upon Total Variation. We recast the problem as a Second-Order Cone Program (SOCP) [18] and solve it by the log-barrier method. Simulation results show that our proposed methodologies can recover the air pollutant concentration map with much higher accuracy compared to traditional approaches.

The rest of this paper is organized as follows. The system model of the prediction of 3D high resolution spatial-temporal air pollutant concentration map is given in Section 2. Section 3 details the proposed algorithms in this paper. Section 4 illustrates the simulation results on real air pollutant data. Finally the conclusions and future works are given in Section 5.

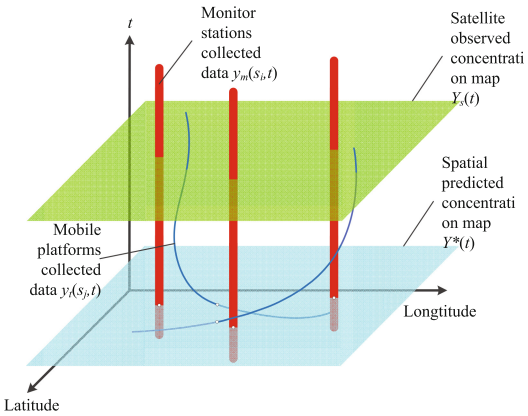

Fig. 2. Illustration of the system model. $y_{\text{mon}}(s_i,t), i = 1,2,...,m$ are the observations from m monitor stations; $y_{\text{taxi}}(s_j,t), j = 1,2,...,n$ are the mobile platforms collected measurements, and the blue curves show their spatial-temporal trajectories; $Y^{*(3)}$ is the preliminarily predicted 3D air pollutant map; $Y_{\text{s}}^{(3)}$ is the satellite observed low-resolution air pollutant concentration map

2 System Model

Consider a system model illustrated in Fig. 2. Since the distribution of ambient air pollutants closely follows a log-normal distribution [16], we use $y(s_l,t)$ to denote the logarithm of the air pollutant concentration measured at station s_l and day t, where $l = 1,...,d, t = 1,...,T$. Among these we have m fixed observations from ground monitor stations and n random observations from mobile platforms(i.e. taxis) with mobile sensing nodes, where $m + n = d$. In other words,

$$\{y(s_l,t)|l = 1,...,d\} = \{y_{\text{mon}}(s_i,t), y_{\text{taxi}}(s_j,t)|i = 1,...,m; j = 1,...,n\}. \quad (1)$$

Then, we model the measurement equation as [8]:

$$y(s_l,t) = \mathbf{x}(s_l,t)\boldsymbol{\beta} + \xi(s_l,t) + \varepsilon(s_l,t), \quad (2)$$

where $\mathbf{x}(s_l,t) = (x_1(s_l,t),...,x_p(s_l,t))$ denotes the vector consists of p covariates for station s_l at time t, and $\boldsymbol{\beta} = (\beta_1,...,\beta_p)'$ is the corresponding coefficient vector. Thus, $\mathbf{x}(s_l,t)\boldsymbol{\beta}$ is regression part in the measurement equation (2), which is also called the large scale component [10][11] that models the dependence of air pollutant concentration on various meteorology and geography covariates.

The residual from the regression is partitioned into a spatial-temporal process, $\xi(s_l,t)$, and a measurement error $\varepsilon(s_l,t) \overset{i.i.d.}{\sim} N(0,\sigma_\varepsilon^2)$ which is defined by a both temporally and spatially uncorrelated Gaussian white-noise process. $\xi(s_l,t)$ is a Gaussian field that consists of a first order auto-regressive dynamics $a\xi(s_l,t-1)$ that models the temporal correlation, and a temporally independent zero-mean Gaussian distribution $\omega(s_l,t)$ that models the spatial correlation.

Thus, $\xi(s_l, t)$ can be formulated as:

$$\xi(s_l, t) = a\xi(s_l, t-1) + \omega(s_l, t), t = 2, ..., T, \tag{3}$$

where $|a| < 1$ is the coefficient of the first order auto-regressive dynamics with $\xi(s_l, 1) \sim N(0, \sigma_\omega^2/(1-a^2))$. Here we set a to a constant under the consideration of the lack of data and computational efficiency.

The spatial correlation item $\omega(s_l, t)$ is characterized by a covariance function:

$$\mathrm{Cov}(\omega(s_l, t), \omega(s_k, t')) = \begin{cases} 0, & \text{if } t \neq t', \\ \sigma_\omega^2 \mathcal{C}(h), & \text{if } t = t'. \end{cases} \quad \text{for } l \neq k. \tag{4}$$

where $h = \parallel s_l - s_k \parallel \in \Re$ is the Euclidean spatial distance between station s_l and s_k, and $\mathcal{C}(h)$ is a function of h defined by a Matérn covariance function [8][17]:

$$\mathcal{C}(h) = \frac{1}{\Gamma(\nu)2^{\nu-1}}(\kappa h)^\nu K_\nu(\kappa h), \tag{5}$$

where K_ν is the modified Bessel function of the second kind with a fixed order $\nu > 0$, which is also the smoothness parameter. And $\kappa > 0$ is the scaling parameter to be estimated [12][14].

Although the above spatial-temporal model has been widely used in the prediction of air pollutant concentrations [9], it has inherent limitations due to the amount direct measurements used. Thus, we propose a brand new model that can combine heterogeneous data sources and provide more reliable prediction results.

3 Proposed Algorithms

In this section, we will first predict a preliminary air pollutant concentration map from the above system model, then model it as well as the low resolution satellite observed concentration data cube in a convex and sparse optimization problem to further improve the accuracy of predicted concentration map.

3.1 Spatial Prediction

Let $\mathbf{y_t} = (y(s_1, t), ..., y(s_d, t))'$ denote all observations measured at time t, then we can rewrite the measurement equations (2)(3) as:

$$\begin{aligned} \mathbf{y_t} &= \mathbf{x_t}\boldsymbol{\beta} + \boldsymbol{\xi_t} + \boldsymbol{\varepsilon_t}, \quad \boldsymbol{\varepsilon_t} \sim N(\mathbf{0}, \sigma_\varepsilon^2 I_d), \\ \boldsymbol{\xi_t} &= a\boldsymbol{\xi_{t-1}} + \boldsymbol{\omega_t}, \quad \boldsymbol{\omega_t} \sim N(\mathbf{0}, \Sigma), \end{aligned} \tag{6}$$

where $\mathbf{x_t} = (\mathbf{x}(s_1, t)', ..., \mathbf{x}(s_d, t)')'$ is the covariance matrix at time t, $\boldsymbol{\xi_t} = (\xi(s_1, t), ..., \xi(s_d, t))'$, and I_d is the d-dimension identity matrix, Σ is the $d \times d$ dense correlation matrix with elements $\Sigma(l, k) = \mathcal{C}(\parallel s_l - s_k \parallel), l, k = 1, ..., d$.

In a Bayesian framework, we will need to estimate the parameter vector $\boldsymbol{\theta} = (\boldsymbol{\beta}, \sigma_{\varepsilon}^2, a, \sigma_{\omega}^2, \kappa)$ given $\mathbf{y} = \{\mathbf{y_t} | t = 1, ..., T\}$, and then make spatial predictions based on $\boldsymbol{\theta}$. According to the Bayes's Rule, the posterior distribution of $\boldsymbol{\theta}$ given $\mathbf{y}$ is:

$$\pi(\boldsymbol{\theta}|\mathbf{y}) \propto \pi(\mathbf{y}|\boldsymbol{\theta})\pi(\boldsymbol{\theta}), \tag{7}$$

where $\pi(\cdot)$ denotes the probability density function.

The common approach for this estimation and prediction is MCMC sampling [9]. However, the computation cost of MCMC is quite heavy, making it almost impossible when it comes to large scale big data sources. In this paper, we will first represent the Gaussian field $\boldsymbol{\xi_t}$ as a GMRF [14], which can be characterized by a sparse precision matrix via the SPDE approach [12]. This allows us to further adopt the INLA algorithm [13] as an alternative of MCMC, which has significantly computational efficiency for the parameter estimation and spatial prediction.

Let $Y^{*(3)}(t)$ denote the spatially predicted air pollutant concentration maps for all $t \in \{1, 2, ..., T\}$, we can build a 3D air pollutant concentration map $Y^{*(3)} = (Y^{*(3)}(1); ...; Y^{*(3)}(T))$. Note that the prediction results are usually based on limited number of samples, so the accuracy of $Y^{*(3)}$ can not be guaranteed. Thus, we will further take advantage from our third data source, the satellite observed low resolution air pollutant concentration map $Y_{\mathrm{s}}^{(3)}$.

3.2 Restoration via Sparse Optimization

Assume that the spatial resolution of each temporal slice $Y^{(3)}(t)$ in the 3D air pollutant concentration map $Y^{(3)}$ is $M \times N$, then we have $Y^{(3)} \in \Re^{M \times N \times T}$. For the ease of notation and computation, we represent the 3D air pollutant data tensor as a matrix $Y \in \Re^{D \times T}$, where $D = M \times N$. Let $\mathbf{e}_t := (0, ..., 1, ..., 0)$ be the column selector with the t-th element being 1 for $t = 1, 2, ..., T$. Thus we can denote the column vectors as $\mathbf{y}_t = Y\mathbf{e}_t$.

We find that for each temporal slice $Y_t^{(3)}$, it is sparse in the sense of small Total Variation [15][18]. Thus, we can formulate the problem of restoring each column y_t in the actual air pollutant concentration matrix Y as:

$$\begin{aligned} \min_{\mathbf{y}_t} \quad TV(\mathbf{y}_t), \quad \text{s.t.} \quad & \| L(\mathbf{y}_t^{(2)}) - Y_{\mathrm{s}}\mathbf{e}_t \|_2 \leq \epsilon_1, \\ & \| K\mathbf{e}_t \cdot \mathbf{y}_t - Y_{\mathrm{r}}\mathbf{e}_t \|_2 \leq \epsilon_2, \\ & \| \mathbf{y}_t - Y^*\mathbf{e}_t \|_2 \leq \epsilon_3. \end{aligned} \tag{8}$$

The physical meaning of each term in the above objective function is listed as follows:

- Total Variation: $TV(\mathbf{y}_t)$ is the Total Variation regularization of $\mathbf{y}_t$, where $TV(\cdot)$ denotes the Total Variation semi-norm;
- Satellite data: $\| L(\mathbf{y}_t^{(2)}) - Y_{\mathrm{s}}\mathbf{e}_t \|_2 \leq \epsilon_1$ is the constraint to keep the greatest similarity possible between $\mathbf{y}_t$ and satellite observed data $Y_{\mathrm{s}}\mathbf{e}_t$, where ϵ_1 is

the error bound. In order to lower resolve each temporal slice $Y^{(3)}(t)$, we use $\mathbf{y}_t^{(2)}$ to denote the matricization of $\mathbf{y}_t$, i.e.,

$$\mathbf{y}_t^{(2)} = Y^{(3)}(t). \tag{9}$$

The operator $L(\cdot)$ is to lower-resolve $\mathbf{y}_t^{(2)}$ to the same size with $Y_\mathrm{s}\mathbf{e}_t$, which is the t-th column in the 2D representation of the satellite data cube $Y_\mathrm{s}^{(3)}$.

- Monitor stations and mobile platforms data: $\| K\mathbf{e}_t \cdot \mathbf{y}_t - Y_\mathrm{r}\mathbf{e}_t \|_2 \leq \epsilon_2$ is the constraint to grantee the actual observed data can be preserved in the restoration result Y, where ϵ_2 is the error bound, and K is the mask matrix has the same size to Y:

$$K(q,t) = \begin{cases} 1, & \text{if there is a measurent,} \\ 0, & \text{otherwise.} \end{cases} \tag{10}$$

Y_r is the matrix marking the real observed data, i.e.,

$$Y_\mathrm{r}(q,t) = \begin{cases} y(s_l,t), & \text{if there is a measurent,} \\ 0, & \text{otherwise,} \end{cases} \tag{11}$$

where is $y(s_l,t)$ is the ground monitor station or mobile platform collected data at the corresponding location, and $q \in \{1,2,...,D\}, t \in \{1,2,...,T\}$.

- Preliminary predicted data: $\| \mathbf{y}_t - Y^*\mathbf{e}_t \|_2 \leq \epsilon_3$ is the constraint to keep the similarity between $\mathbf{y}_t$ and the t-th column of preliminarily predicted data $Y^*\mathbf{e}_t$, and ϵ_3 is the error bound.

For the ease of computation, we first rewrite the above optimization equation (8) as follows:

$$\min_{\mathbf{y}_t} \quad TV(\mathbf{y}_t), \quad \text{s.t.} \quad \| A(\mathbf{y}_t) - b \|_2 \leq \epsilon, \tag{12}$$

where

$$A(\mathbf{y}_t) = \begin{pmatrix} L(\mathbf{y}_t^{(2)}) \\ K\mathbf{e}_t \cdot \mathbf{y}_t \\ \mathbf{y}_t \end{pmatrix}, b = \begin{pmatrix} Y_\mathrm{s}\mathbf{e}_t \\ Y_\mathrm{r}\mathbf{e}_t \\ Y^*\mathbf{e}_t \end{pmatrix}, \tag{13}$$

and ϵ is the total error bound. We can further recast equation (12) as a standard SOCP [18] problem via introducing an intermediate variable z:

$$\begin{aligned} \min_{z} \quad \sum_{u,v=1}^{D} z, \quad \text{s.t.} \quad & \| V_{uv}\mathbf{y}_t \|_2 \leq z, \quad u,v = 1,...,D, \\ & \| A(\mathbf{y}_t) - b \|_2 \leq \epsilon, \end{aligned} \tag{14}$$

where $V \in \Re^{D\times D}$ is the matrix form of finite difference, i.e. $V\mathbf{y}_t = TV(\mathbf{y}_t)$, and D is the length of $\mathbf{y}_t$. Then we can easily solve (14) via the log-barrier method [19].

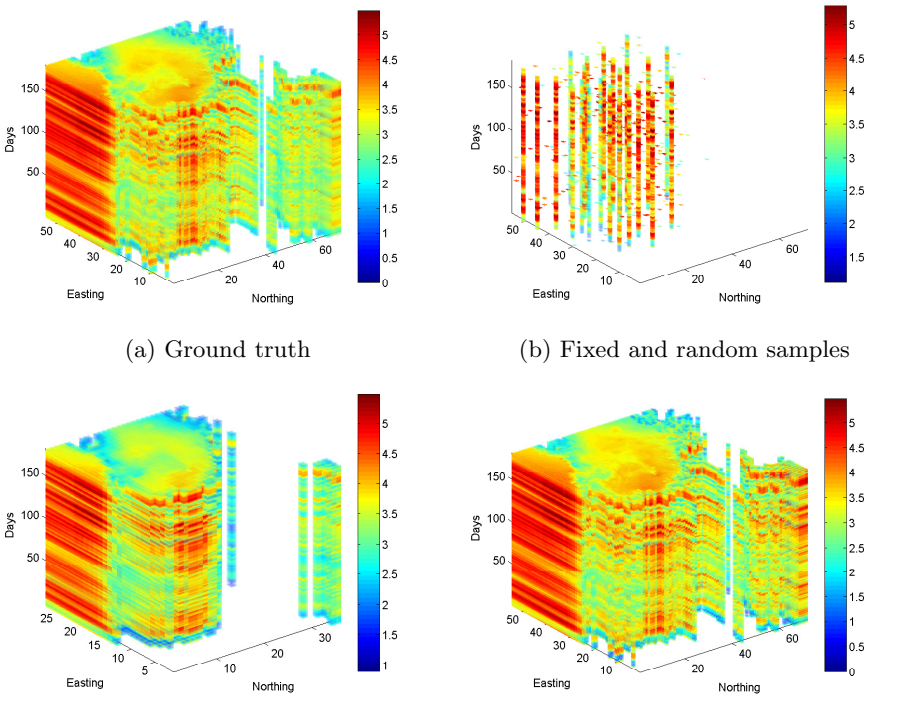

(a) Ground truth (b) Fixed and random samples

(c) Satellite data (PSNR=8.0468dB) (d) Restoration result (PSNR=37.3714dB)

Fig. 3. Simulation results

4 Simulation Results

We use the data set provided by [8] for our simulations, which is the daily PM10 concentration for the Piemonte area in Italy. The data set contains a total $T = 182$ days during the winter season from October 2005 to March 2006. The meteorology covariates taken in to consideration are: daily mean temperature (TEMP, K), daily maximum mixing height (HMIX, m), daily mean wind speed (WS, m/s), daily precipitation (P, mm) and daily emissions (EMI, g/s); the geography covariates taken in to cosidertaion are altitude (A, m) and spatial geographic coordinates (UTMX and UTMY, km).

In order to give a complete assessment of the performance of our proposed algorithm, we first perform a spatial prediction on the data set in [8] via the SPDE-INLA approach to get a 3D concentration map, which we treat as the ground truth as shown in Fig. 3a. We disregard the area with elevations above $1km$ in this concentration map, because there is a mountain in that region and has no monitor stations, thus the prediction result is not reliable. Then we sample from the ground truth map for 24 fixed measurements and 2 random measurements each day to serve as the labeled data, as shown in Fig. 3b. The parameter

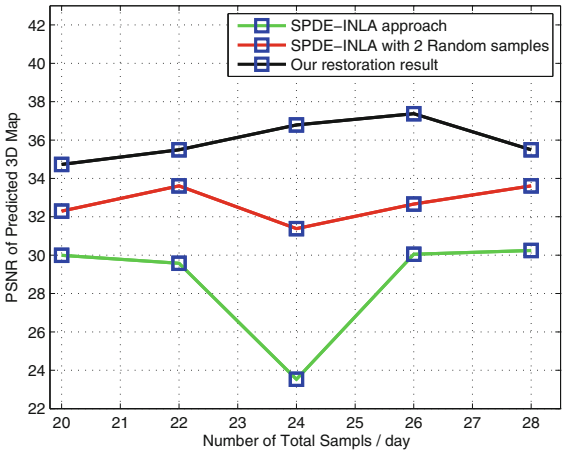

Fig. 4. PSNR curve for different number of samples

estimation and spatial prediction mentioned in Section 3.1 are based on these labeled data. We use the lower resolved ground truth data as satellite data shown in Fig. 3c, which has a very low Peak Signal-to-Noise Ratio (PSNR) of 8.0468dB. Finally we perform the algorithm in Section 3.2 to further improve the accuracy of the predicted concentration data. The restoration result is shown in Fig. 3d. We use PSNR of as the evaluation result instead of the traditional cross validation over several points. The PSNR of our restored concentration map is 37.3714dB, which shows a significant improvement.

The curves in Fig. 4 show the PSNR for different numbers of samples. The green curve is the PSNR of the prediction result using the SPDE-INLA approach in [8] with all measurements fixed. The significant decline at 24 samples is due to the inappropriately choosed samples. The red curve is the prediction result of SPDE-INLA approach with 2 fixed samples replaced by random ones, and it proves that mobile platform observations can help improve the prediction accuracy. Finally, the black curve is the prediction result of our proposed restoration algorithm. It shows that our proposed methodology, i.e. taking random samples and satellite data into consideration, can significantly improve the accuracy of the predicted air pollutant concentration map.

5 Conclusions

In this paper, we take advantage from heterogeneous big data sources to predict a high resolution and accuracy air pollutant concentration map. The final prediction result is the achieved by a spatial prediction via the SPDE-INLA approach and an optimization model based on Total Variation sparse assumptions. With 24 fixed samples and 2 random samples each day and some meteorology and geography covariates, we can improve the PSNR of low-resolution satellite data from 8.0468dB to 37.3714dB. Simulation results validate the efficiency of our algorithm.

References

1. WHO Air Pollution Estimates; WHO (2014)
2. Manyika, J., Chui, M., Brown, B., Bughin, J., Dobbs, R., Roxburgh, C., Angela, H.B., McKinsey Global Institute: Big data: The next frontier for innovation, competition, and productivity (2011)
3. Zhu, Y., Hinds, W.C., Kim, S., Sioutas, C.: Concentration and size distribution of ultrafine particles near a major highway. Journal of the air & waste management association **52**(9), 1032–1042 (2002)
4. Hasenfratz, D., Saukh, O., Walser, C., Hueglin, C., Fierz, M., Thiele, L.: Pushing the spatio-temporal resolution limit of urban air pollution maps. In: 2014 IEEE International Conference on Pervasive Computing and Communications (PerCom), pp. 69–77. IEEE, Budapest, March 2014
5. Hoek, G., Beelen, R., de Hoogh, K., Vienneau, D., Gulliver, J., Fischer, P., Briggs, D.: A review of land-use regression models to assess spatial variation of outdoor air pollution. Atmospheric Environment **42**(33), 7561–7578 (2008)
6. Ryan, P.H., LeMasters, G.K.: A review of land-use regression models for characterizing intraurban air pollution exposure. Inhalation Toxicology **19**(S1), 127–133 (2007)
7. Zheng, Y., Liu, F., Hsieh, H.P.: U-Air: when urban air quality inference meets big data. In: Proceedings of the 19th ACM SIGKDD International Conference on Knowledge Discovery and Data Mining, pp. 1436–1444. ACM, Chicago, August 2013
8. Cameletti, M., Lindgren, F., Simpson, D., Rue, H.: Spatio-temporal modeling of particulate matter concentration through the SPDE approach. AStA Advances in Statistical Analysis **97**(2), 109–131 (2013)
9. Cameletti, M., Ignaccolo, R., Bande, S.: Comparing spatio-temporal models for particulate matter in Piemonte. Environmetrics **22**(8), 985–996 (2011)
10. Cressie, N.A., Cassie, N.A.: Statistics for spatial data, vol. 900. Wiley, New York (1993)
11. Cressie, N., Wikle, C.K.: Statistics for spatio-temporal data. John Wiley & Sons (2011)
12. Lindgren, F., Rue, H., Lindstrm, J.: An explicit link between Gaussian fields and Gaussian Markov random fields: the stochastic partial differential equation approach. Journal of the Royal Statistical Society: Series B (Statistical Methodology) **73**(4), 423–498 (2011)
13. Rue, H., Martino, S., Chopin, N.: Approximate Bayesian inference for latent Gaussian models by using integrated nested Laplace approximations. Journal of the royal statistical society: Series b (statistical methodology) **71**(2), 319–392 (2009)
14. Rue, H., Held, L.: Gaussian Markov random fields: theory and applications. CRC Press (2005)
15. Rudin, L.I., Osher, S., Fatemi, E.: Nonlinear total variation based noise removal algorithms. Physica D: Nonlinear Phenomena **60**(1), 259–268 (1992)
16. Limpert, E., Stahel, W.A., Abbt, M.: Log-normal Distributions across the Sciences: Keys and Clues. BioScience **51**(5), 341–352 (2001)
17. Matérn covariance function - Wikipedia, the free encyclopedia. http://en.wikipedia.org/wiki/Mat%C3%A9rn_covariance_function
18. Goldfarb, D., Yin, W.: Second-order cone programming methods for total variation-based image restoration. SIAM Journal on Scientific Computing **27**(2), 622–645 (2005)
19. Boyd, S., Vandenberghe, L.: Convex optimization. Cambridge University Press (2004)